

G.Tresset, D.Moreau, X.Litaudon, X.Garbet and JET EFDA Contributors

# Characterization of Internal Transport Barriers in JET and Simulations of Control Algorithms

---



# Characterization of Internal Transport Barriers in JET and Simulations of Control Algorithms

G.Tresset, D.Moreau, X.Litaudon, X.Garbet and JET EFDA Contributors\*

<sup>1</sup>*Association Euratom-CEA, CE Cadarache, 13108 St Paul-lez-Durance Cedex, France.*

<sup>2</sup>*Euratom-UKAEA Fusion Association, Culham Science Centre, Abingdon, U.K.*

*\*See appendix of the paper by J.Pamela "Overview of recent JET results",  
Proceedings of the IAEA conference on Fusion Energy, Sorrento 2000*

Preprint of Paper to be submitted for publication in Proceedings of the  
EPS Conference,  
(Madeira, Portugal 18-22 June 2001)

“This document is intended for publication in the open literature. It is made available on the understanding that it may not be further circulated and extracts or references may not be published prior to publication of the original when applicable, or without the consent of the Publications Officer, EFDA, Culham Science Centre, Abingdon, Oxon, OX14 3DB, UK.”

“Enquiries about Copyright and reproduction should be addressed to the Publications Officer, EFDA, Culham Science Centre, Abingdon, Oxon, OX14 3DB, UK.”

## ABSTRACT

The analysis of experiments performed at various magnetic field intensities pointed to an apparent magnetic-field-dependent power threshold for the emergence of ITBs in regions of weak positive magnetic shear in JET [1]. This observation motivated our search for an objective existence criterion which could possibly lead to a better understanding and quantification of the physical processes leading to the formation of ITBs. Furthermore, there is a real interest in developing some physical and practical criterion which could be used routinely to speed up the ITB identification and characterise their main features especially for database analysis, and possibly to control their dynamics in real-time. The first section introduces the criterion, its physical and experimental relevance. In section 2, we use the criterion to investigate the role of the q-profile in the ITB physics for various injected torques. Finally, in the last section, algorithms for profile control using the real-time estimate of the criterion are proposed and numerically simulated.

## 1. A DIMENSIONLESS CRITERION FOR ITB CHARACTERISATION

The physical mechanisms of barrier formation have not yet been completely identified, but drift waves are thought to be the principal vector of microturbulence when the plasma is driven far from thermodynamic equilibrium, and their stabilisation is likely to be the cause of a transport reduction leading to the emergence of ITBs [2]. Despite a variety of possible unstable modes, a fundamental characteristic length arises from their dispersion relations: the ion Larmor radius at the sound speed,  $\rho_s = c_s/\omega_{ci}$ , where  $c_s$  is the ion sound speed, and  $\omega_{ci}$  the ion cyclotron pulsation. When transport barriers appear, local gradient scale lengths become much shorter than the plasma size and, for a local analysis, one should indeed normalise the drift wave scale length  $\rho_s$  to the local temperature gradient scale, e.g.  $L_T = -T / (\delta T/\delta R)$  where T is either the ion or electron temperature and R is the plasma major radius on the equatorial plane. We therefore define the local dimensionless Larmor radius,  $\rho_T^*$ , as  $\rho_T^* = \rho_s/L_T$ . When considering various experimental scenarios with different plasma currents and, more importantly, with a wide range of heating powers and magnetic field intensities, it is worth testing whether an ITB existence criterion could possibly be expressed according to the local value of  $\rho_T^*$ . Noting that the simplest dimensionless criterion would read:

$$\rho_T^*(R, t) = -\frac{1}{Z_i} \sqrt{\frac{m_i}{e}} \frac{\sqrt{T_e}}{B_\phi} \frac{1}{T} \frac{\partial T}{\partial R} \stackrel{?}{=} \rho_{ITB}^* \Leftrightarrow \text{an ITB exists at radius R and time t}$$

$Z_i$  and  $m_i$  are the ion charge number and mass respectively,  $e$  the elementary charge,  $B_\phi$  the toroidal magnetic field and all the temperatures are expressed in keV. The critical dimensionless number  $\rho_{ITB}^*$ , if it does exist, should depend only on a few dimensionless parameters and can be evaluated experimentally. Further developments introducing a treatment of measurement uncertainties as well as a plausible theoretical relevance of the above criterion based on the stabilising effect of the E×B shear rate can be found in [3].

The critical value  $\rho_{ITB}^*$  was chosen from a discharge with a perfectly visible barrier whose emergence time was well defined and which was used as a reference. It was thus

found that  $\rho_{\text{ITB}}^* \approx 1.4 \times 10^{-2}$  would match both the emergence time and radial evolution of the barrier satisfactorily in JET. Pulses obtained with almost the same operating conditions but which either exhibit an ITB or not were also compared and successfully distinguished by the  $\rho_{\text{T}}^* \geq 1.4 \times 10^{-2}$  criterion.

An attractive representation of the results is obtained by plotting contours of  $\rho_{\text{T}}^*$  in the  $(t, \rho)$  plane,  $\rho$  the normalised radius. The constant- $\rho_{\text{T}}^*$  contours are plotted only for  $\rho_{\text{T}}^* \geq \rho_{\text{ITB}}^*$ . Figure 1 shows an example of such a graph for a discharge where the ITB dynamics is rich of events. It can be seen that all the relevant information such as onset time, collapse times, as well as the dynamics and width of the barrier appear explicitly for a low computational cost.

In order to evaluate its reliability for detecting the presence and evolution of ITBs, our criterion was tested on many discharges from the JET database with various experimental conditions. For this purpose 116 deuterium pulses were selected with toroidal magnetic fields varying from 1.8 to 4T, plasma currents from 1.6 to 3.6MA (safety factors from 3.3 to 4.3), central densities from 2 to  $5.5 \times 10^{19} \text{ m}^{-3}$ , NBI powers from 4.8 to 18.7MW and ICRH powers from 0 to 8.7MW. It must be noted that mostly electron temperature barriers were considered here because of the good spatial and temporal resolutions of the ECE diagnostic. Among these 116 discharges, 84 presented an ITB. Their emergence times were then evaluated by identifying a divergence between temperature traces from neighbouring radii and are confronted with the  $\rho_{\text{Te}}^*$  criterion on Fig. 2. Only five very weak barriers were not detected by the criterion whereas one detection was not assessed by a detailed data analysis.

## 2. ROLE OF THE Q-PROFILE AND INJECTED TORQUE IN THE ITB PHYSICS

Discharges where the ITB regime was established with either monotonic or reversed shear q-profiles are analysed with our criterion. In these experiments, described in [4], the injected torque has been varied systematically for each q-profile by selecting either dominantly tangential bank beam, or dominantly normal bank beam or mainly on-axis ion cyclotron heating (at  $B_{\Phi} = 2.6\text{T}$  and  $I_p = 2.2\text{-}2.3 \text{ MA}$ ). Hollow q-profiles are obtained at the start of the main heating phase by coupling 2MW of LHCD during the current ramp-up phase. The main applied heating consists of a combination of NBI and ICRH powers. Figure 3 shows the maximal value of  $\rho_{\text{Te}}^*$  versus the total additional power for different q-profile and injected torque. At a given power and injection configuration, the pulses with LH preheat expected to have an inverted q-profile, confirmed by both polarimetry and MSE data, exhibit a better ITB quality than without any preheat (monotonic q-profile). As the ITBs are located roughly at the same radius ( $\rho \approx 0.5\text{-}0.6$ ) close to the  $q = 2$  surface, this result demonstrates an improvement of barrier performances as the magnetic shear lowers. Furthermore, for the same q-profile, the ITB strength seems to decrease with lower injected torque or fuelling, the poorest performances being with ICRH. This figure also shows that the access power of  $q = 2$  electron ITBs varies from 9MW with large applied torque up to 12MW with dominant ICRH. We investigate now the role of the q-profile in ITB triggering. The q-profile was determined here with the magnetic reconstruction code EFIT constrained by infrared polarimetry data. For the 11 pulses presenting a

clear ITB in these experiments, the safety factor value at the barrier onset time and location is  $2 \pm 0.08$ . This phenomenon is depicted on Fig. 4 where two pulses with the same applied torque but different q-profile shapes are confronted. Figure 4(a) shows that an ITB is formed only when the  $q = 2$  surface enters the plasma even though the main heating has started for several fast ion slowing down and thermal confinement times. On the contrary, a barrier is formed earlier on Fig. 4(b) possibly due to the presence of the  $q = 2$  surface. For the case of monotonic q-profiles, the role of the rational surfaces has been discussed in [5]. Our analysis confirms that ITBs emerge close to rational q surface and preferentially in weak magnetic shear regions. This is consistent with the drop of turbulence observed numerically when the density of resonant surfaces decreases [6].

### 3. MODELLING OF FEEDBACK CONTROL FOR ADVANCED SCENARIOS

The inherent simplicity in its expression makes the proposed ITB criterion well-suited for real-time control application, a crucial issue to achieve the so-called advanced tokamak regime. In this last section, we present transport modelling of real-time feedback algorithms based on the normalised gradient  $\rho_{Te}^*$ . In a steady-state operation, maintaining an ITB consists in supplying a sufficient amount of energy into the plasma to overcome the local turbulence, while avoiding dangerous MHD instabilities especially those related to pressure peaking. Mostly two quantities have been numerically studied as response signals for a real-time feedback loop: i) the maximal value over radii of the dimensionless Larmor radius  $(\rho_{Te}^*)_{max}$ , ii) the total neutron rate  $R_{nt}$ . The actuators, i.e. the sources of energy, are either the NBI or ICRH powers. A Proportional-Integral (PI) feedback algorithm has been implemented as follows:

$$P(t) = P(t_0) + G_p DX(t) + G_I \int_{t_0}^t \Delta X(u) du \text{ with } \Delta X(t) = X_{ref} - X(t)$$

where  $t_0$  denotes the time at which control is turned on,  $P$  the required power,  $X$  the feedback signal,  $G_p$  and  $G_I$  are the proportional and integral gains respectively. The latter are of great importance for an optimal response of the system. Figure 5 pictures a simulation of a double feedback control scheme performed with the transport code ASTRA [7]. The feedback on  $(\rho_{Te}^*)_{max}$  by ICRH at its reference value allows to sustain the barrier and the control on  $R_{nt}$  by NBI prevents potential disruptive events. Such simulations have allowed to prepare real-time control experiments in JET [8] by testing various schemes, and optimising the combination of actuators and gains.

### ACKNOWLEDGEMENTS

Thanks are due to Dr. G. Pereverzev for the use of the ASTRA code.

### REFERENCES

- [1]. C.Gomezano, Plasma Phys. Control. Fusion 41 (1999) B367.
- [2]. W.Horton, Rev. Mod. Phys. 71 (1999) 735.
- [3]. G.Tresset et al., Report EFDA-JET-PR(00)09, Nov. 2000, submitted to Nucl. Fusion.
- [4]. C.D.Challis et al., these proceedings.

- [5]. E.Joffrin et al., submitted to Nucl. Fusion.
- [6]. X.Garbet et al., Phys. Plasmas 8 (2001) 2793.
- [7]. G.Pereverzev et al., Report IPP 5/42, IPP Garching (Germany) 1991.
- [8]. D.Mazon et al., these proceedings.



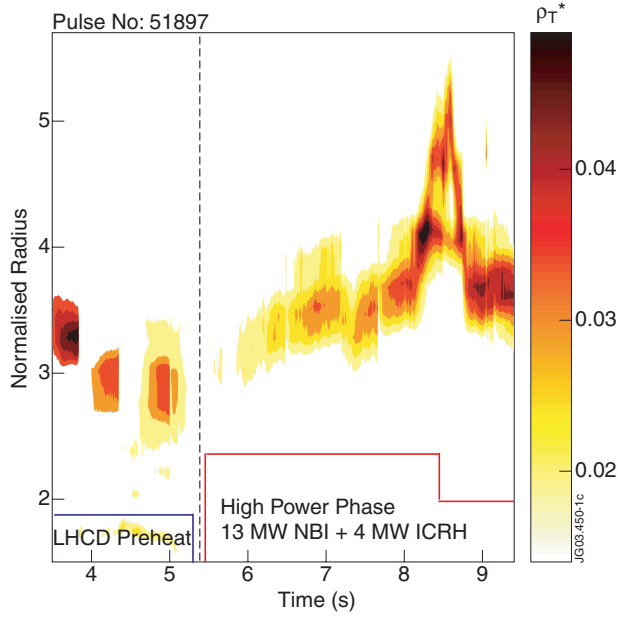


Figure 1: Constant- $\rho_{Te}^*$  contours plotted for  $\rho_{Te}^* \geq \rho_{ITB}^*$  showing the space-time evolution of an electron ITB (Pulse No: 51897).

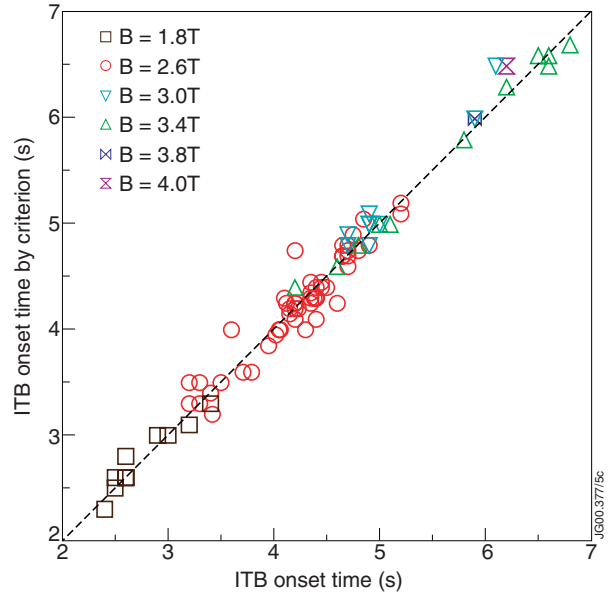


Figure 2: Statistics on the validation of the ITB emergence time through the  $\rho_{Te}^*$  criterion for various magnetic field intensities. The emergence time determined by  $\rho_{Te}^* = \rho_{ITB}^*$  is plotted against that determined independently from data analysis.

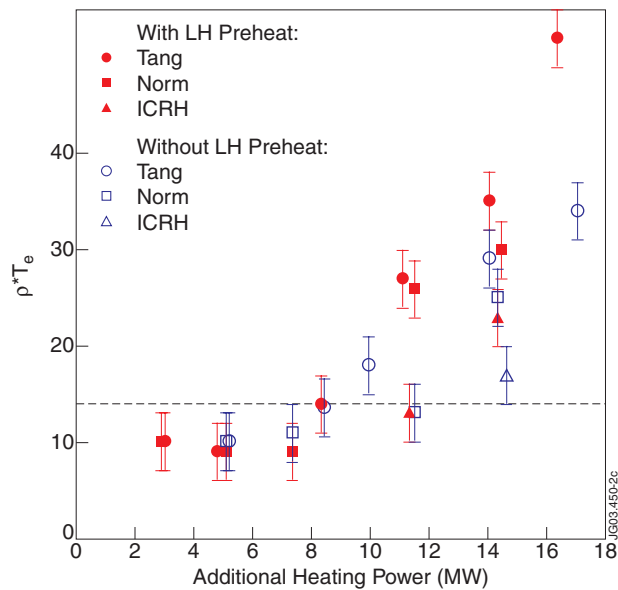


Figure 3: Maximal value of  $\rho_{Te}^*$  versus total additional heating power for various injection configurations and with or without LHCD prelude. The horizontal dashed line indicates the criterion threshold value  $\rho_{ITB}^*$ .

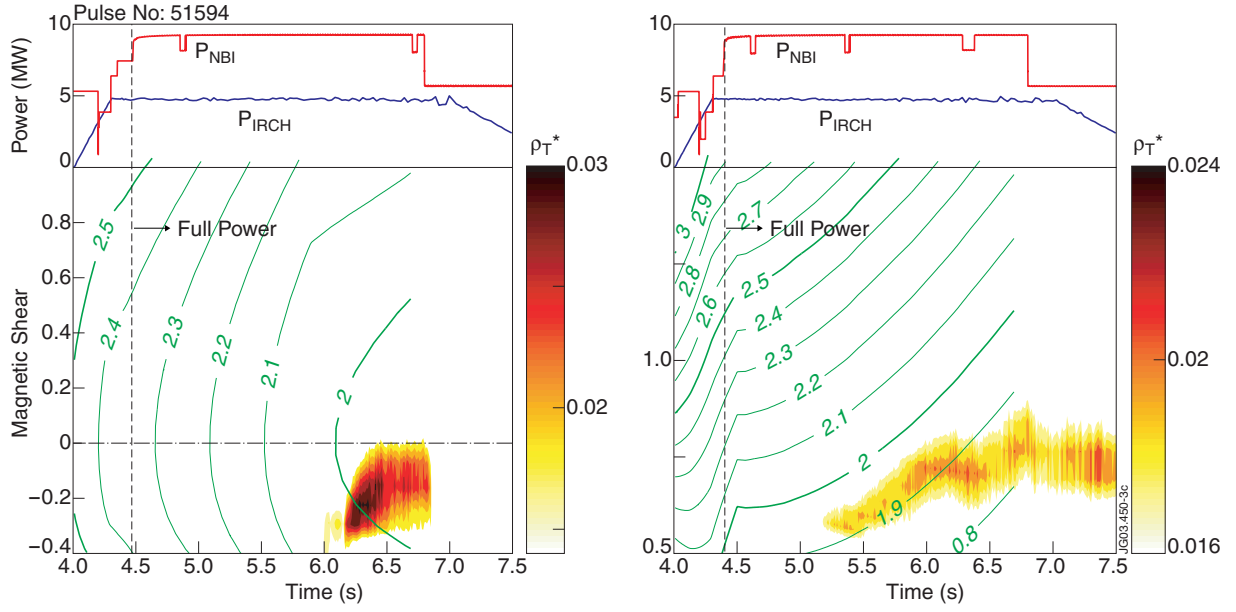


Figure 4: a) (left) Constant- $\rho_{Te}^*$  ( $\rho_{Te}^* \rho_{ITB}^*$ ) contours in the plane  $(s,t)$ ,  $s$  magnetic shear, superimposed with constant- $q$  contours.  $B_\phi = 2.6T$ ,  $I_p = 2.2MA$ ,  $P_{add} = 14MW$  (tangential beams) and  $2.3MW$  of LH preheat (Pulse No: 51594). b) (right) Constant- $\rho_{Te}^*$  contours in the plane  $(s,t)$  superimposed with constant- $q$  contours.  $B_\phi = 2.6T$ ,  $I_p = 2.2MA$ ,  $P_{add} = 14MW$  (tangential beams) and no LH preheat (Pulse No: 51595).

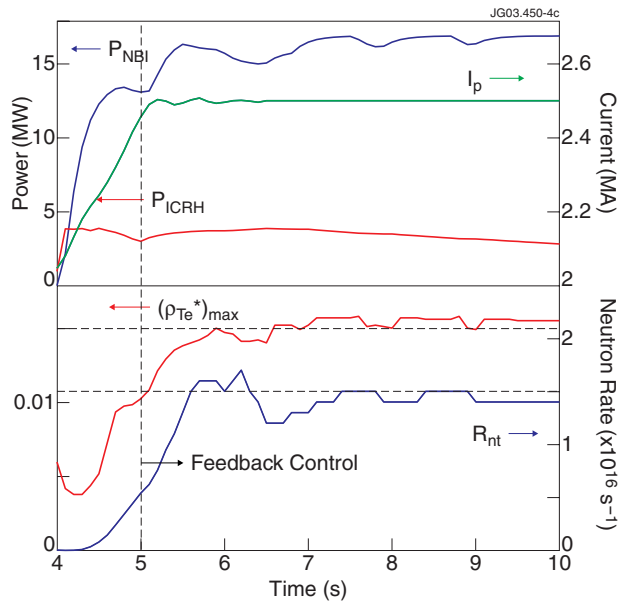


Figure 5: Simulation of a double feedback control scheme on  $(\rho_{Te}^*)_{max}$  and  $R_{nt}$  by  $P_{ICRH}$  and  $P_{NBI}$  respectively using a PI algorithm.  $B_\phi = 2.5T$ ,  $I_p = 2.5MA$ ,  $(G_I/G_p)_{ICRH} = 25 \cdot \delta t$ ,  $(G_I/G_p)_{NBI} = 5 \cdot \delta t$  and  $\delta t = 10ms$ . The horizontal dashed lines show the reference values (Pulse No: 46123 before control).